



Lawrence Berkeley Laboratory

UNIVERSITY OF CALIFORNIA

Materials Sciences Division

Submitted to the Journal of the Electrochemical Society

Simulation and Optimization of the Dual Lithium Ion Insertion Cell

T.F. Fuller, M. Doyle, and J. Newman

May 1993



Prepared for the U.S. Department of Energy under Contract Number DE-AC03-76SF00098

LOAN COPY
Circulates
for 4 weeks

Bldg. 50 Library.
Copy 2

LBL-33426

DISCLAIMER

This document was prepared as an account of work sponsored by the United States Government. While this document is believed to contain correct information, neither the United States Government nor any agency thereof, nor the Regents of the University of California, nor any of their employees, makes any warranty, express or implied, or assumes any legal responsibility for the accuracy, completeness, or usefulness of any information, apparatus, product, or process disclosed, or represents that its use would not infringe privately owned rights. Reference herein to any specific commercial product, process, or service by its trade name, trademark, manufacturer, or otherwise, does not necessarily constitute or imply its endorsement, recommendation, or favoring by the United States Government or any agency thereof, or the Regents of the University of California. The views and opinions of authors expressed herein do not necessarily state or reflect those of the United States Government or any agency thereof or the Regents of the University of California.

LBL-33426
UC-331

Simulation and Optimization of the
Dual Lithium Ion Insertion Cell

Thomas F. Fuller, Marc Doyle, and John Newman

Department of Chemical Engineering
University of California

and

Materials Sciences Division
Lawrence Berkeley Laboratory
University of California
Berkeley, California 94720

May 1993

This work was supported in part by the Assistant Secretary for Conservation and Renewable Energy, Office of Transportation Technologies, Electric and Hybrid Propulsion Division of the U. S. Department of Energy under Contract No. DE-AC03-76SF00098.

Simulation and Optimization of the Dual Lithium Ion Insertion Cell

Thomas F. Fuller, Marc Doyle, and John Newman

Abstract

The galvanostatic charge and discharge of a dual lithium ion insertion ("rocking-chair") cell are modeled. Transport in the electrolyte is described with concentrated solution theory. Insertion of lithium into and out of the active electrode material is simulated using superposition, greatly simplifying the numerical calculations. Simulation results are presented for the Li_xC_6 |propylene carbonate+1M LiClO_4 | $\text{Li}_y\text{Mn}_2\text{O}_4$ cell, and these results are compared with experimental data from the literature. Criteria are established to assess the importance of diffusion in the solid matrix and of transport in the electrolyte. Various procedures to optimize the utilization of active material are considered. Simulation results for the dual lithium ion insertion cell are compared with those for a cell with a solid lithium negative electrode.

Introduction

The storage and conversion of energy continues to be important to society. Batteries, which interconvert chemical and electrical energy, are widely used in industry and for consumer applications (e.g., appliances and lap-top computers). At the same time, environmental concerns are reshaping many industries. The ecological hazards of batteries through their operation and disposal is a primary consideration for manufacturers of batteries. In addition, stricter emission standards on automobiles are spurring interest in batteries for electric-vehicle applications. The energy and power requirements for vehicle propulsion are rigorous.¹ Consequently, research on rechargeable battery systems is receiving renewed attention.

Lithium batteries are attractive for the storage of energy because of their high theoretical energy densities. Furthermore, they are less toxic than nickel cadmium or lead acid cells, and their disposal poses fewer environmental problems. Although primary lithium batteries have been mass-produced for years,² the secondary (rechargeable) lithium cell has only recently been commercialized.^{3,4,5} The typical lithium cell is made up of a lithium metal negative electrode, an electrolyte which serves as an ionic path between electrodes and separates the two materials, and a positive electrode, such as Mn_2O_4 .

In general, a highly reactive material is desired for the negative electrode to give a higher cell potential, and hence a higher theoretical energy density. Unfortunately, the more reactive the electrode material the more likely it will react irreversibly with the electrolyte. The high reactivity of the lithium metal is a significant problem

for lithium batteries. Successful lithium battery systems are able to operate due to a protective film that forms on the electrode surface.⁶ This protective film retards further reaction with the electrolyte but impacts the capacity and cycle life of the cell through increased resistance and material isolation. The highly reactive lithium metal is a safety issue as well, becoming especially important in larger cells.

One alternative scheme has been to replace the lithium metal negative electrode with a lithium alloy or compound, such as: LiAl ,⁷ LiFe_2O_3 ,⁸ LiWO_2 ,⁸ or LiC_6 .⁹ Although these materials stabilize the lithium, this reduces the energy density of the cell, since the added material is not used in the operation of the system. Even with this drawback, several lithium batteries have been developed using this strategy.

Rechargeable batteries for electric-vehicle applications require long cycle life; 500 to 1000 cycles is desired before the capacity falls below 80% of its initial value. For this to be possible, the electrochemical reactions must be highly reversible. Some of the most reversible electrodes operate through insertion reactions. In these electrodes, commonly layered transition metal oxides, the ionic species is transported across the electrolyte and diffuses between the layers or in interstitial sites of the electrode structure where it is stabilized by favorable coulombic interactions. Because there is no bond breaking or appreciable restructuring of the electrode during this process, the mechanism is highly reversible. A general discussion of the insertion process has been given by Whittingham.^{10,11} Hundreds of materials that insert lithium ions reversibly have been developed and tested since

their usefulness for battery applications was recognized.¹²

Some years ago it was realized that replacing the lithium metal with another insertion material was a possible solution to the high reactivity and irreversibilities of the solid lithium negative electrode.¹³ This material would have to insert lithium at a potential that is appreciably lower than that of the positive electrode; in effect, it should have less favorable energetics for the insertion process. The cell potential results from differences in the activity of lithium in the two insertion materials. The operation of the system would then involve the shuttling of lithium ions back and forth between the two insertion compounds, and hence has sometimes been given the colloquial name "rocking-chair" cell.¹⁴ These systems will have a lower energy density than those with solid lithium as discussed above. The reversibility and improved safety of these systems makes them attractive nonetheless. Several companies have recently announced their intentions to bring rechargeable batteries based on this concept to market.^{4,5} More background on the conceptual development of the dual insertion battery is given by Scrosati.²

The development of a detailed mathematical model is important to the design and optimization of lithium secondary cells and critical in their scale-up. West *et al.*¹⁵ treated insertion into a composite cathode consisting of an active insertion material and electrolyte in a porous structure, but did not consider a full cell. A more complete model of a lithium-anode, solid-polymer-electrolyte, porous-insertion-cathode cell was given by Doyle *et al.*¹⁶ Simulation results for a lithium metal anode, polyethylene oxide separator, and TiS_2 composite

cathode, including discharge curves and concentration profiles, are provided.

Our objective here is to develop a general model of the dual insertion cell. Given the physical properties and system parameters, the model can simulate any particular choice of materials. This model is then used to evaluate the performance of a specific system, and the simulation results are compared with experimental discharge curves obtained from the literature. In particular, we are able to assess the importance of diffusion in the solid material, which is thought to be a limitation in some cells. Different applications may require different rates of discharge. This model allows us to evaluate the suitability of various systems for these applications. Finally, the optimization of the performance of these cells will be discussed.

Model Development

We have modeled the galvanostatic charge and discharge of the cell sandwich shown in figure 1. We consider one-dimensional transport of lithium ions from the negative electrode through the separator into the positive electrode. The composite electrodes consist of an inert conducting material, the electrolyte, and the solid active insertion particles. The theory derives from work of Newman¹⁷ and from the preceding model of Doyle *et al.*¹⁶ Consequently, only the salient features of the model will be given here. We will focus instead on the discussion of simulation results and optimization issues.

Transport in the separator is modeled with concentrated solution theory, assuming a binary electrolyte and solvent. With three species

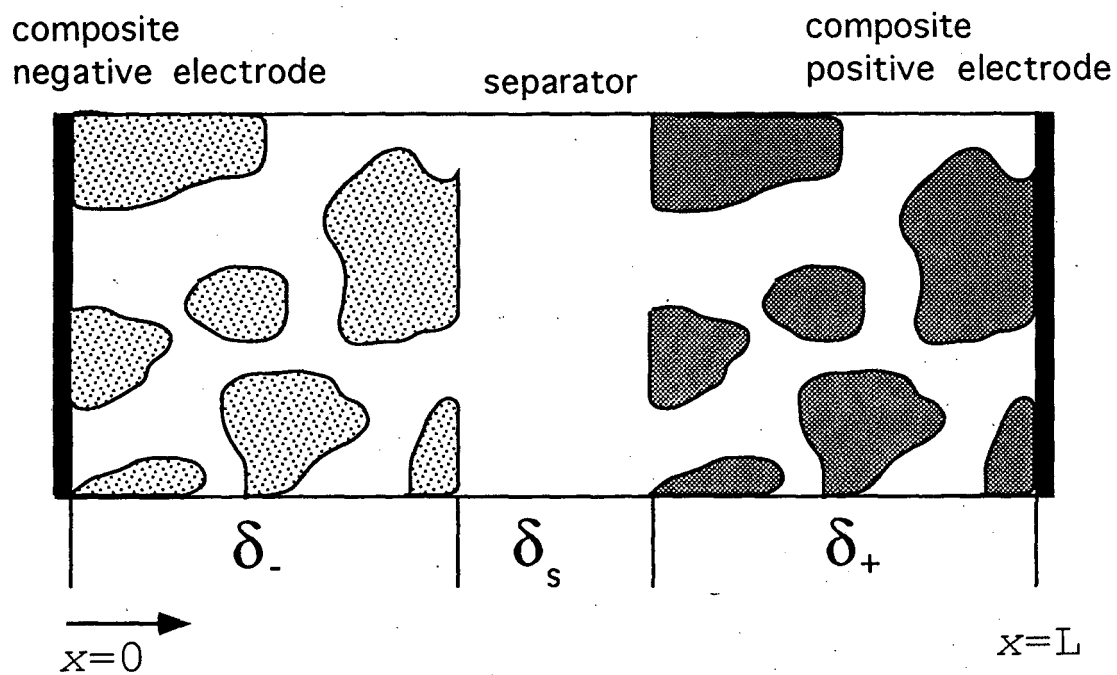


Figure 1. Dual-insertion cell sandwich, consisting of composite negative and positive electrodes, and separator.

(e.g., Li^+ , X^- , and solvent), the electrical conductivity, the transfer number of the lithium ion, and the diffusion coefficient of the lithium salt characterize transport in the electrolyte. This macroscopic approach, using concentrated solution theory with variable physical properties, allows one to deal rigorously with the transport phenomena.

In concentrated solution theory, the driving force for mass transfer is the gradient in electrochemical potential.

$$c_i \nabla \mu_i = \sum_{j \neq i} K_{ij} (\mathbf{v}_j - \mathbf{v}_i), \quad (1)$$

where the K_{ij} ($K_{ij} = K_{ji}$) are frictional coefficients describing interactions between species i and j . For a solution of a binary salt plus solvent, because of the Gibbs-Duhem equation, we have two independent transport equations of the form given in equation 1. If we use the solvent as the reference species and take its velocity to be zero, we can invert these equations to obtain:

$$N_+ = -\nu_+ D \nabla c + \frac{it_+^0}{z_+ F} \quad (2)$$

and

$$N_- = -\nu_- D \nabla c + \frac{it_-^0}{z_- F} \quad (3)$$

c is the concentration of the electrolyte ($c = c_i / \nu_i$). The K_{ij} 's can be related directly to the three measurable transport properties D , t_+^0 , and

κ. 16-18

A material balance on the electrolyte gives

$$\epsilon \frac{\partial c}{\partial t} = \nabla \cdot (\epsilon D \nabla c) - \frac{i_2 \cdot \nabla t_+^0}{z_+ \nu_+ F} + \frac{a j_n (1 - t_+^0)}{\nu_+}, \quad (4)$$

where ϵ is the volume fraction of the electrolyte. We have assumed that the porosity is constant and that volume changes can be neglected. j_n is the pore wall flux across the interface between the electrolyte and the active material. This pore wall flux is averaged over the interfacial area between the solid matrix and the electrolyte. Thus, the last term can be viewed as a reaction rate per unit volume, and equation 4 is analogous to the treatment of a packed-bed reactor.

The current in the two phases is conserved;

$$I = i_1 + i_2. \quad (5)$$

The total current, I , is uniform and flows through either the electrolyte phase (i_2) or through the insertion material phase (i_1). The current flowing in the matrix is governed by Ohm's law;

$$i_1 = -\sigma \nabla \Phi_1. \quad (6)$$

The variation of potential in the electrolyte is¹⁷

$$i_2 = -\kappa \nabla \Phi_2 + \frac{\kappa RT}{F} \left(1 + \frac{\partial \ln f_{\pm}}{\partial \ln c} \right) (1 - t_+^0) \nabla \ln c, \quad (7)$$

where Φ_2 is measured with a lithium reference electrode in solution.

Equation 7 is similar to Ohm's law but includes a term for concentration variations. The pore wall flux, j_n , is related to the divergence of the current flow in the electrolyte phase through Faraday's law,

$$aj_n = \frac{-s_i}{nF} \nabla \cdot i_2. \quad (8)$$

Boundary conditions for equations 4, 6, and 7 derive from the condition that the flux density of each ionic species must be zero at the ends of the cell. From this, we obtain the conditions that

$$\nabla c = 0 \text{ at } x=0 \text{ and } x=L.$$

At the ends of the cell, we can also say that the current flows in the solid matrix only ($i_2 = 0$). Thus from equations 5 and 6, we find

$$\nabla \Phi_1 = -I/\sigma \text{ at } x=0 \text{ and } x=L. \quad (9)$$

Because we are interested only in potential differences, we arbitrarily set the potential in the solution phase to zero at $z=L$; for galvanostatic behavior, we specify the current ($I = i_2$) in the separator.

In porous media, transport properties must be modified to account for the actual path length of the species.¹⁹ Therefore in the composite electrodes,

$$\kappa_{eff} = \kappa \epsilon^{1.5},$$

and

$$D_{eff} = D\epsilon^{0.5}$$

The active electrode material is assumed to be made up of spherical particles of radius R_s with diffusion being the mechanism of transport of the lithium into the particle. The model is also able to simulate cylindrical and planar particles of given size; the treatment is analogous. We take the direction normal to the surface of the particles to be the r -direction. Thus,

$$\frac{\partial c_s}{\partial t} = D_s \left[\frac{\partial^2 c_s}{\partial r^2} + \frac{2}{r} \frac{\partial c_s}{\partial r} \right], \quad (10)$$

where c_s represents the concentration of lithium in the solid particle phase. From symmetry,

$$\frac{\partial c_s}{\partial r} = 0 \text{ at } r=0. \quad (11)$$

The second boundary condition is provided by a relationship between the pore wall flux across the interface and the rate of diffusion of lithium ions into the surface of the insertion material,

$$j_n = -D_s \frac{\partial c_s}{\partial r} \text{ at } r=R_s. \quad (12)$$

As the diffusion coefficient of the inserted lithium ions has been assumed constant, this is a linear problem and can be solved by the method of superposition²⁰ (see appendix B). In brief, we can calculate the flux at the surface of the insertion particles from the prior surface concentrations and a series of coefficients, which are calculated

separately.

The open-circuit potential of insertion materials varies with the amount of lithium inserted and is expressed by a general function of composition in the particle,

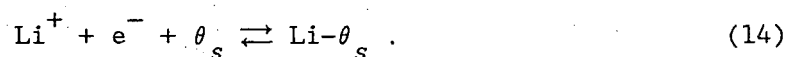
$$U = U^\theta - U_{ref}^\theta + F(c_s). \quad (13)$$

The function $F(c_s)$ can vary widely depending on the insertion chemistry of the material. For example, lithium inserts into TiS_2 between layers of sulfur atoms, held together by weak van der Waals forces, forming a continuous phase that is salt like. There is a small change in free energy with the amount of lithium inserted, and the cell potential decreases slowly with lithium content. On the other hand, insertion into manganese dioxide causes a distortion in the crystal lattice. This electrode has an open-circuit potential that exhibits two plateaux corresponding to the thermodynamic potentials of each phase transition. By definition, compounds such as the manganese dioxide that exhibit phase changes during discharge are not true insertion materials, as insertion is a nonstoichiometric process that should not involve formation of a specific phase. However, for the purposes of this model even compounds that have phase changes will be treated as insertion materials. Our model is general and any continuous function can be used for the open-circuit potential above.

There are limited data available on the kinetics of the charge-transfer reaction at the surface of insertion compounds. Pollard and Newman²¹ have shown that the assumption of infinitely fast kinetics for a porous electrode will lead to a spike in the local current density at

the separator/electrode interface at short times. Assuming infinitely fast kinetics also changes the governing equations. We wish to keep the model general so that the kinetics of the electrodes can be included if data are available. Consequently, a charge-transfer resistance will be considered in the present model. Due to a lack of data, the values used for the exchange current densities at the insertion material surfaces will correspond to highly reversible charge-transfer processes.

For a general charge-transfer reaction from a liquid electrolyte, the following form is assumed for the insertion process;



Here θ_s represents a site in the solid insertion material. If the kinetics follow a Butler-Volmer form,[‡]

$$j_n = k(c)^{\alpha_a} (c_t - c_s)^{\alpha_a} (c_s)^{\alpha_c} \left\{ \exp\left[\frac{\alpha_a F}{RT}(\eta-U)\right] - \exp\left[-\frac{\alpha_c F}{RT}(\eta-U)\right] \right\} \quad (15)$$

Here k represents the product of the forward and backward rate constants, each raised to a power depending on the transfer coefficients, for the charge-transfer reaction at the electrode surface. The overpotential η is defined as

$$\eta = \Phi_1 - \Phi_2 \quad (16)$$

Equations 4, 6, 7, 8, 10, and 12 are linearized and solved simultaneously using the subroutine BAND.¹⁷ We have two independent

‡ For the carbon electrode $0.5c_t$ was used in place of c_t .

variables (x and t) and six dependent variables (c , Φ_2 , c_s , i_2 , j_n , and Φ_1). The Crank-Nicolson implicit method was used to evaluate the time derivatives.

Results and Discussion

Appendix A gives transport properties for the electrolyte and thermodynamic data for each electrode. We modeled a cell consisting of a carbon negative electrode, lithium perchlorate in propylene carbonate liquid electrolyte, and manganese dioxide positive electrode. The lithium perchlorate/propylene carbonate electrolyte in the separator region of the cell was assumed to be confined to the voids of an inert polymer material such as polypropylene. The inert separating material is assumed to have a constant void fraction of 0.4, and transport properties of the electrolyte in this region are adjusted accordingly. The carbon material was petroleum coke, with the composition range for lithium insertion being $0 < x < 0.5$, that used by Guyomard and Tarascon.²²

It should be mentioned that the optimum solvent for this system is not propylene carbonate alone, but rather a mixed solvent system. These solvent mixtures allow a more reversible insertion process at the carbon electrode⁹ and have been demonstrated to exhibit better conductivities.²³ However, reliable values of the lithium ion transference number and salt diffusion coefficient do not exist for these systems. We simulated propylene carbonate alone because the transport properties for this solvent are known. Even for lithium perchlorate in propylene carbonate, the variations of the transport properties with concentration are incomplete. For this reason, the concentration dependence of the

conductivity is the only variable physical property included in these simulations.

Additional parameters used in this model are listed in tables 1 and 2. The quantities in table 1 are inherent properties of the specific system and are determined from experimental measurement. On the other hand, quantities in table 2 can be varied to optimize a particular battery design. These adjustable parameters, where possible, have been chosen to correspond to those used by Guyomard and Tarascon,²² permitting a comparison with their experimental results.

The high electronic conductivity used for the two electrodes is that obtained with a small fraction of conducting material (carbon black) added to the solid matrix. We did not wish to consider the effects of low electronic conductivity on the discharge behavior, as this is an unnecessary complication that would be avoided in practical systems. The volume fraction of conducting filler added to each electrode was chosen to correspond to that used by Guyomard and Tarascon.²² The maximum concentrations in the positive and negative electrodes are estimated from the density of the material at composition LiMn_2O_4 or LiC_6 , respectively. z is the capacity ratio of the positive to negative electrode;

$$z = \frac{c_{t,+}(1-\epsilon_+ - \epsilon_{f,+})\delta_+}{c_{t,-}(1-\epsilon_- - \epsilon_{f,-})\delta_-} \quad (17)$$

Figure 2 shows the cell potential as a function of utilization of positive electrode material for galvanostatic charge and discharge for the carbon/manganese dioxide cell. The state of charge is measured with

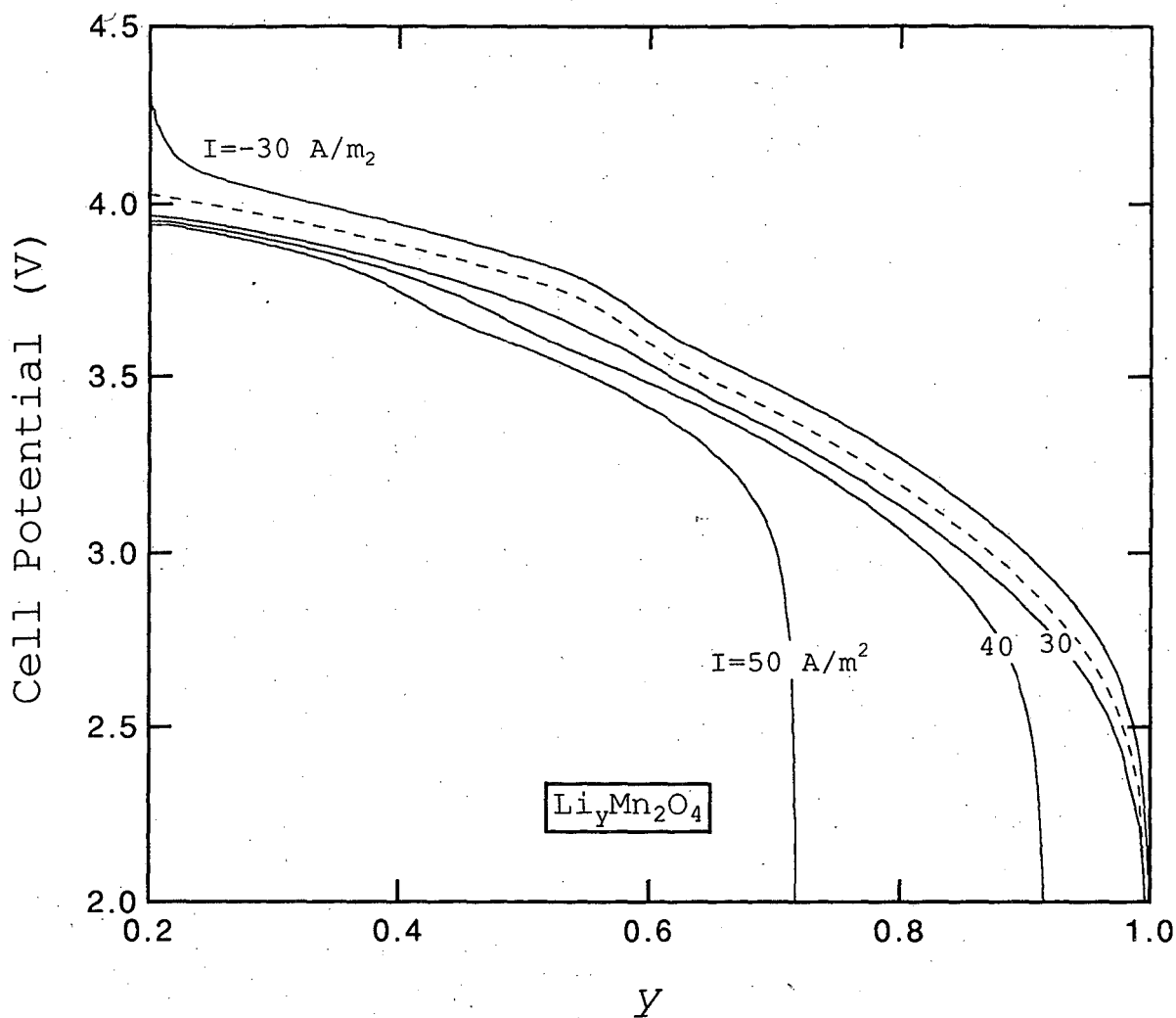


Figure 2. Cell potential versus state of discharge for the manganese dioxide/carbon system at various discharge rates. The dashed line is the open-circuit potential of the cell. Other parameters used in the simulation are given in tables 1 and 2.

Table 1.
Parameters for the electrodes

parameter	$\text{Li}_y\text{Mn}_2\text{O}_4$	Li_xC_6
D_s (m^2/s)	10^{-13} [22]	5.0×10^{-13} [22]
σ (S/m)	100	100
i_o (A/m^2)	2.89‡	0.41‡
α_c, α_a	0.5	0.5
c_t (mol/m^3)	23,720	26,400
ρ_s (kg/m^3)	4100	1900

Table 2.
Design adjustable parameters

parameter	$\text{Li}_y\text{Mn}_2\text{O}_4$	Li_xC_6
δ_+, δ_- (μm)	200	243
R_s (μm)	1	18
c_s^o (mol/m^3)	4744	13,070
ϵ	0.3	0.3
ϵ_f	0.151	0.044
parameter	value	
T ($^\circ\text{C}$)	25	
c^o (mol/m^3)	1000	
δ_s (μm)	50	
z	0.62	

y , the stoichiometry of the positive electrode. The manganese dioxide electrode is assumed to insert lithium over the range ($0.2 < y < 1.0$); hence, the initial solid concentration is 20% of the total, or maximum, concentration. For this system y varies between 1 and 0.2, and x varies

‡ Assumed value at initial conditions.

between 0 and 0.495. x and y are related through the capacity ratio z .

$$z = \frac{\Delta x}{\Delta y}. \quad (18)$$

The dashed line represents the open-circuit potential calculated from equations in appendix A, and the current density is a parameter.

The cell potential for this system during discharge at 40 A/m^2 is predicted to be approximately 3.95 V at the start of discharge and decreases to about 3.06 V at $y=0.8$. This is the same range exhibited by cells discharged by Guyomard and Tarascon.²² At higher current densities, ohmic losses are larger, and the cell potential is lower irrespective of concentration polarization. It is apparent that the material utilization is limited at higher discharge rates. For this system, the abrupt drop in cell potential at the higher discharge rates is caused by concentration polarization, as will be discussed further below. We show that at current densities above approximately 40 A/m^2 the utilization of active material begins to drop off for this particular system. This discharge rate is comparable to that obtained by Guyomard and Tarascon²² for manganese dioxide systems of similar thicknesses (see figure 17 of the cited reference). It should be stressed that the above authors were not using a porous electrode, so their system should sustain lower rates of discharge (because of solid-state diffusion).

The concentration of the electrolyte over the time scale of a full discharge is depicted in figure 3 for a current of 40 A/m^2 . Initially the concentration is uniform at 1000 mol/m^3 . Li deinserts from the carbon electrode and inserts into the manganese dioxide electrode on discharge. Since the perchlorate anions are not involved in the

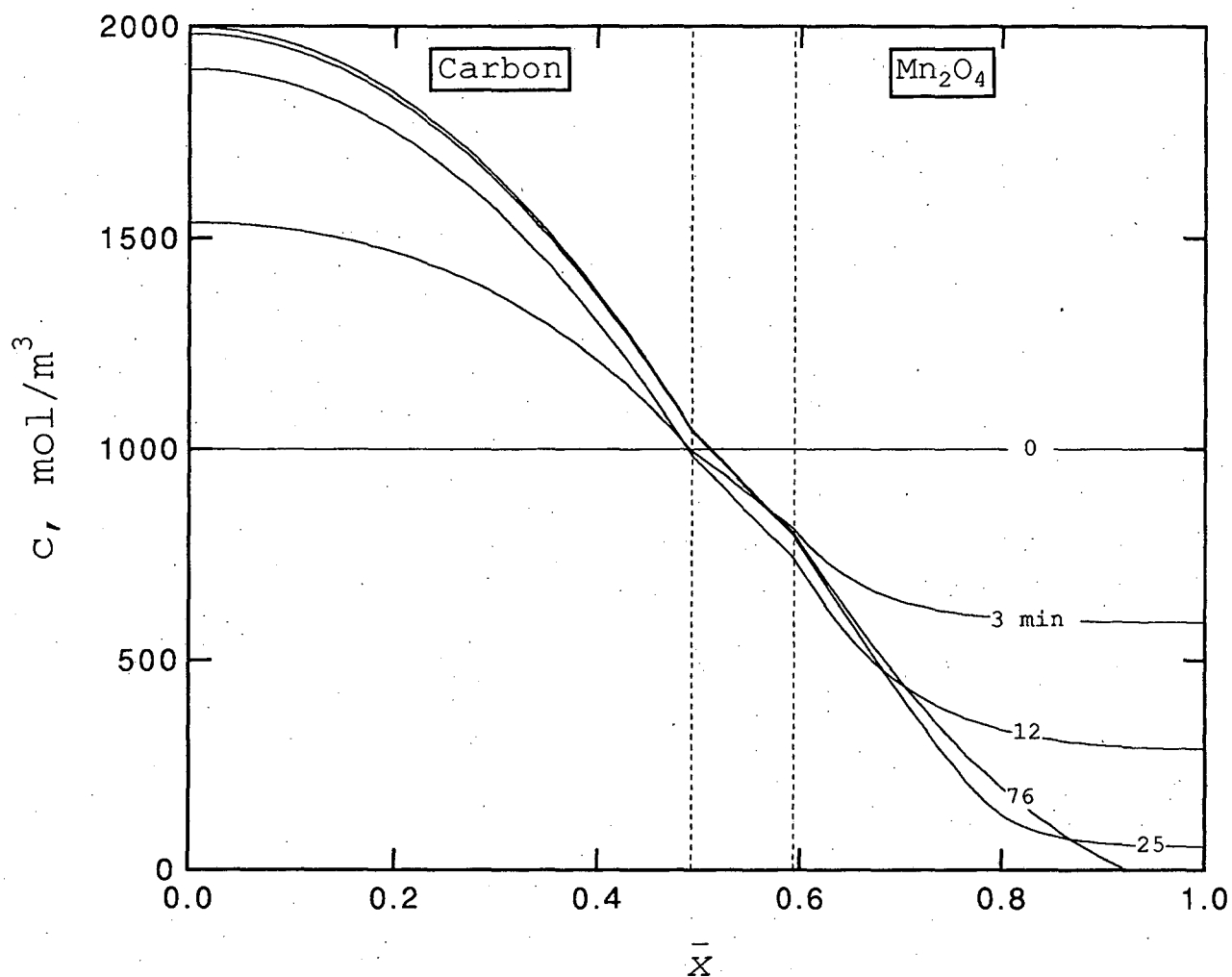


Figure 3. Concentration profiles across cell during galvanostatic discharge at $I = 40 \text{ A/m}^2$. Carbon negative electrode is 21.5% thicker than the manganese dioxide positive electrode. The separator region is set off by dashed lines.

electrochemical reactions, their flux would be zero at steady state. A concentration gradient builds up to balance the migration of anions. This gradient is seen clearly from equation 3. The concentration profile is established quickly in comparison to the time of discharge. Near the end of discharge (76 minutes), the concentration of the electrolyte at the back of the manganese dioxide electrode is driven to zero, a limiting-current phenomenon. Once this happens, the active manganese dioxide material in this region can no longer be used because there are no lithium ions in the solution phase to insert. At higher current densities, the electrolyte concentration would be driven to zero closer to the separator, thus preventing 100% utilization of the electrode. At current densities lower than 40 A/m^2 , a limiting current is never reached.

An important factor in optimizing the performance of the cell is good utilization of the active material. For a specified battery performance, one should like the cell potential to fall below its cutoff value only after nearly all the active material is consumed. This requires an understanding of the transport limitations in each phase of the composite electrodes, as these lead to nonuniform reaction distributions.

The importance of diffusion in the solid electrode material can be assessed from the dimensionless parameter S_s ;

$$S_s = \frac{R_s^2 I}{D_s n F (1 - \epsilon - \epsilon_{f,c}) (c_t - c_s^0) \delta_+} \quad (19)$$

and is the ratio of diffusion time to discharge time. Here the

diffusion time is calculated based on the maximum concentration in the solid and the range of y during cycling. If the positive electrode is not limiting, equation 19 would have to be modified to reflect the time of discharge. For $S_s \ll 1$, diffusion can be neglected. For the dual insertion systems, there will be a different value of this parameter for each electrode. Substitution of the parameters from table 1 into equation 19 with $I=40 \text{ A/m}^2$ gives $S_s \approx 0.002$ for the manganese dioxide electrode and $S_s \approx 0.129$ for the carbon electrode. Thus, diffusion limitations are not expected to exist in the manganese dioxide particles, but they may exist in the carbon. Therefore, for the manganese dioxide particles the concentration at the surface and the average concentration in the solid are nearly identical, and we do not present concentration profiles in the solid.

A typical concentration profile in a solid carbon particle is presented in figure 4. This particle is located near the carbon electrode/separator boundary, and the profile is taken close to the end of discharge. Since the shape of the profiles do not change significantly over the course of discharge for this simulation, this profile is a good representation of the extent of diffusion limitations in the solid particles. The concentration gradient inside the carbon particles is fairly small, about ten percent of the average concentration in the particle. This is in good agreement with the value of S_s calculated above for the carbon particles.

We can also use S_s to predict the radius of the particles for which severe diffusion limitations will exist in the solid phase for this system. We find that diffusion limitations begin, i.e. $S_s=1$, when the man-

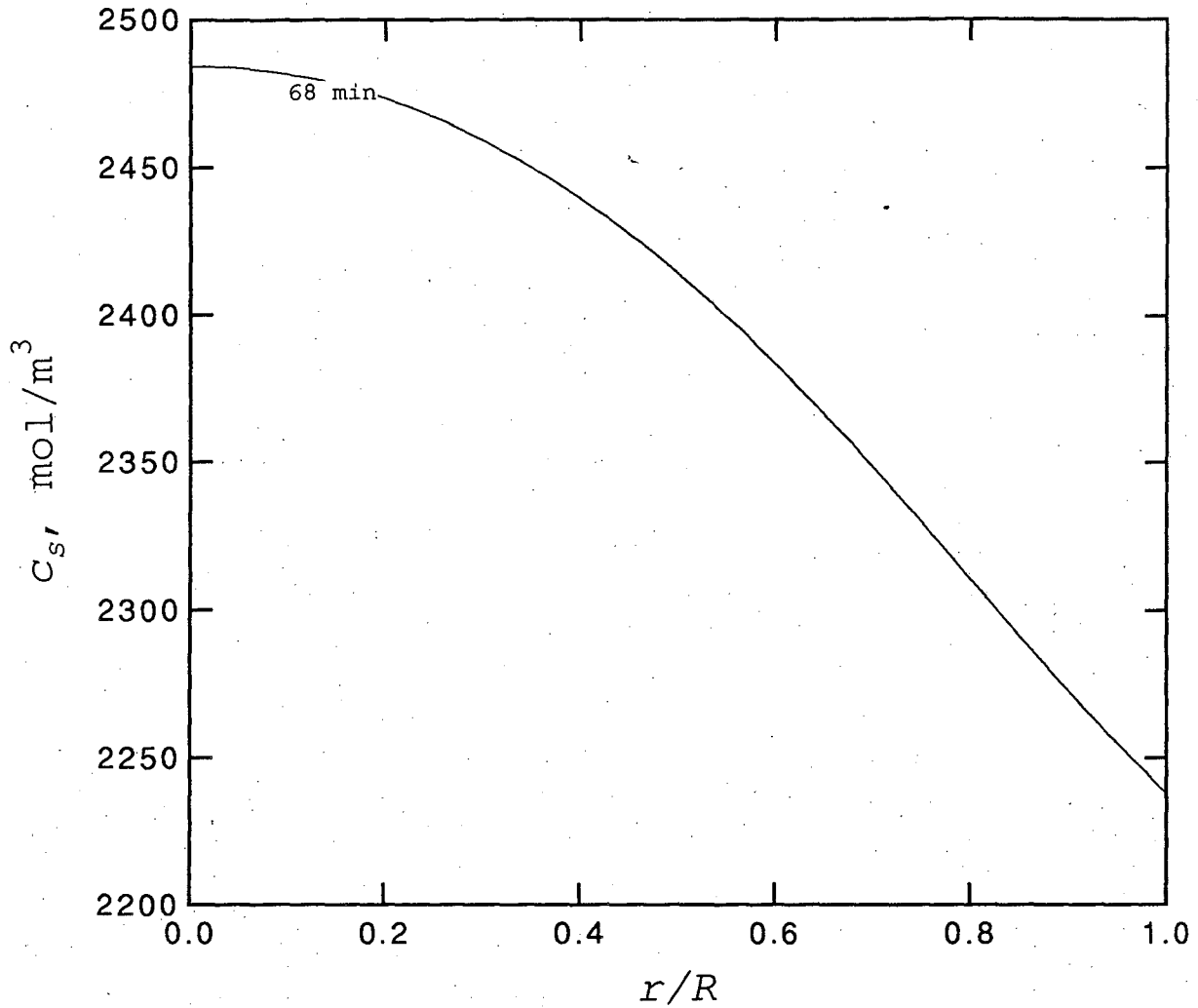


Figure 4. Concentration of lithium inside a solid carbon particle. The discharge rate is $I=40 \text{ A/m}^2$, and the time since the beginning of discharge is 68 minutes. The particle is located at $x=0.4$, near the negative electrode/separator boundary.

ganese dioxide particle radius exceeds 24 μm . This is especially relevant to nonporous electrode structures, where the solid-phase diffusion length is often on this order. Calculating the value of S_s for the nonporous manganese dioxide electrode (thickness of 170 μm) used in Guyomard and Tarascon's²² work, one finds that $S = 37$. As $S > 1$, we should expect that this is the main factor limiting the utilization of material at high rates of discharge in their system.

An analogous parameter can be calculated relating the time constant for transport of the electrolyte to the time of the discharge;

$$S_e = \frac{L^2 I}{DnF(1-\epsilon-\epsilon_{f,c})(c_t - c_s^0)\delta_+} \quad (20)$$

For $I=40 \text{ A/m}^2$, we find that $S_e=0.187$. This explains why the concentration profile in figure 3 is established quickly compared to the discharge time. Because the time for transport in the electrolyte may be small in comparison to the discharge time, steady-state transport limitations must be considered.

In fact, transport limitations in the electrolyte phase are the main factor limiting the performance of this cell at high rates of discharge. The mechanism of failure is the depletion of the electrolyte in the solution phase, which leads to a large concentration overpotential. This would be less of a problem with larger values of the salt diffusion coefficient, the initial salt concentration, or the lithium ion transference number. At higher discharge rates, the concentration in the solution phase can be driven to zero well before 100% utilization has been attained, leading therefore to incomplete utilization of the

active material.

As this is the major cause of the end of discharge, it suggests that increasing the electrolyte concentration would improve the performance of the system at high rates of discharge. The value of the initial concentration used in these systems is generally chosen to correspond to a conductivity maximum. This can be seen for the present system in the figures given in reference 23, where the concentration dependence of the conductivity for this system was obtained. Thus, increasing the concentration above this maximum will lead to an increase in the ohmic drop in the system. However, as has been stressed before,¹⁶ the advantages in terms of the increased concentration in the depth of the porous electrode generally outweigh the increase in ohmic drop. This can be demonstrated by simulating the system at a high rate of discharge corresponding to $I=50 \text{ A/m}^2$ with the initial concentration as a parameter. The results, in the form of discharge curves, are presented in figure 5. Even a small increase in the initial concentration brings about a marked improvement in the attainable utilization. When the initial concentration is increased by 40%, almost complete utilization is obtained.

It should be mentioned that raising the initial concentration also leads to much higher concentrations in the negative electrode on discharge, which may cause problems in lithium salt/solvent systems that have a solubility limit. The maximum concentration attained by the system can be checked using the current model to ensure that a solubility limit is not surpassed. For instance, the solubility limit of lithium perchlorate in propylene carbonate at room temperature is given as 2100

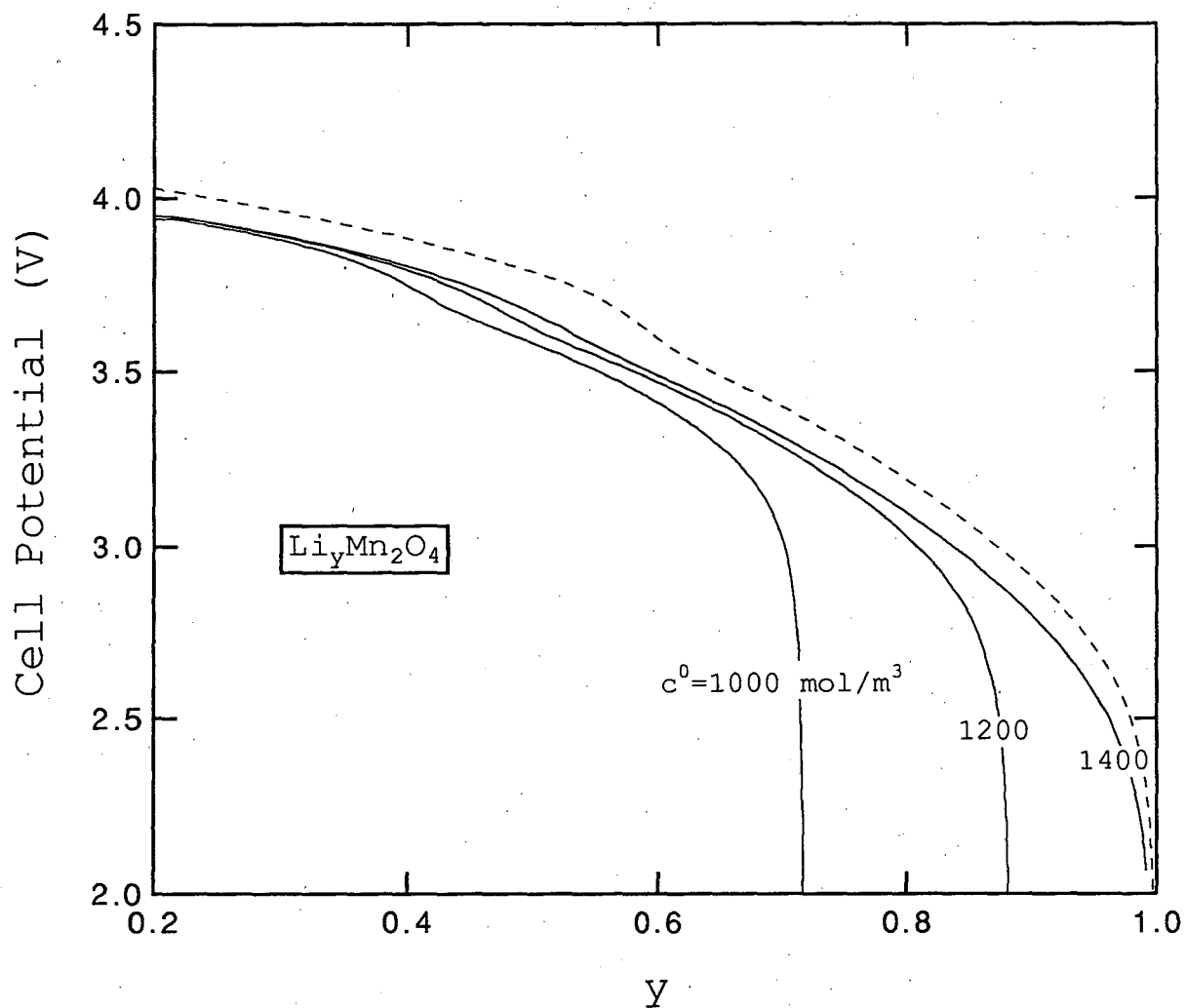


Figure 5. Cell potential versus state of discharge for the manganese dioxide/carbon system with the initial electrolyte concentration as a parameter. The dashed line is the open-circuit potential of the cell. The discharge rate is $I=50$ A/m².

mol/m^3 .²³ Concentrations above this are obtained in the negative electrode for current densities of greater than 50 A/m^2 . This model does not presently account for salt precipitation, but this is an undesirable situation that should be avoided in practice. For the present system, the concentration dependence of the conductivity, but not the transference number and diffusion coefficient, are included (appendix A). To model correctly the possible benefits of increasing the initial concentration in the system further, all these concentration dependences should be included, as well as a consideration of solubility limitations.

Figure 6 shows the divergence of the solution-phase current, which is proportional to the reaction rate per unit volume, across the cathode at various times during discharge. This figure is analogous to a current distribution on the surface of an electrode. The shape of the curves is in general complex, depending on ohmic resistance, electrode kinetics, open-circuit potential, and any transport limitations that exist. Newman¹⁷ gives four dimensionless parameters that characterize the current distribution in a porous electrode. These parameters describe the balance between ohmic and kinetic limitations, but not concentration effects. At short times, the concentration of electrolyte is nearly constant, and these parameters can be used to describe the current distribution. An analysis of this sort has been carried out in an earlier paper¹⁶ and will not be repeated here.

Predicting the current distribution at long times is more difficult. Not only will the depletion of the electrolyte cause concentration polarization to occur, but also it will affect the kinetic expres-

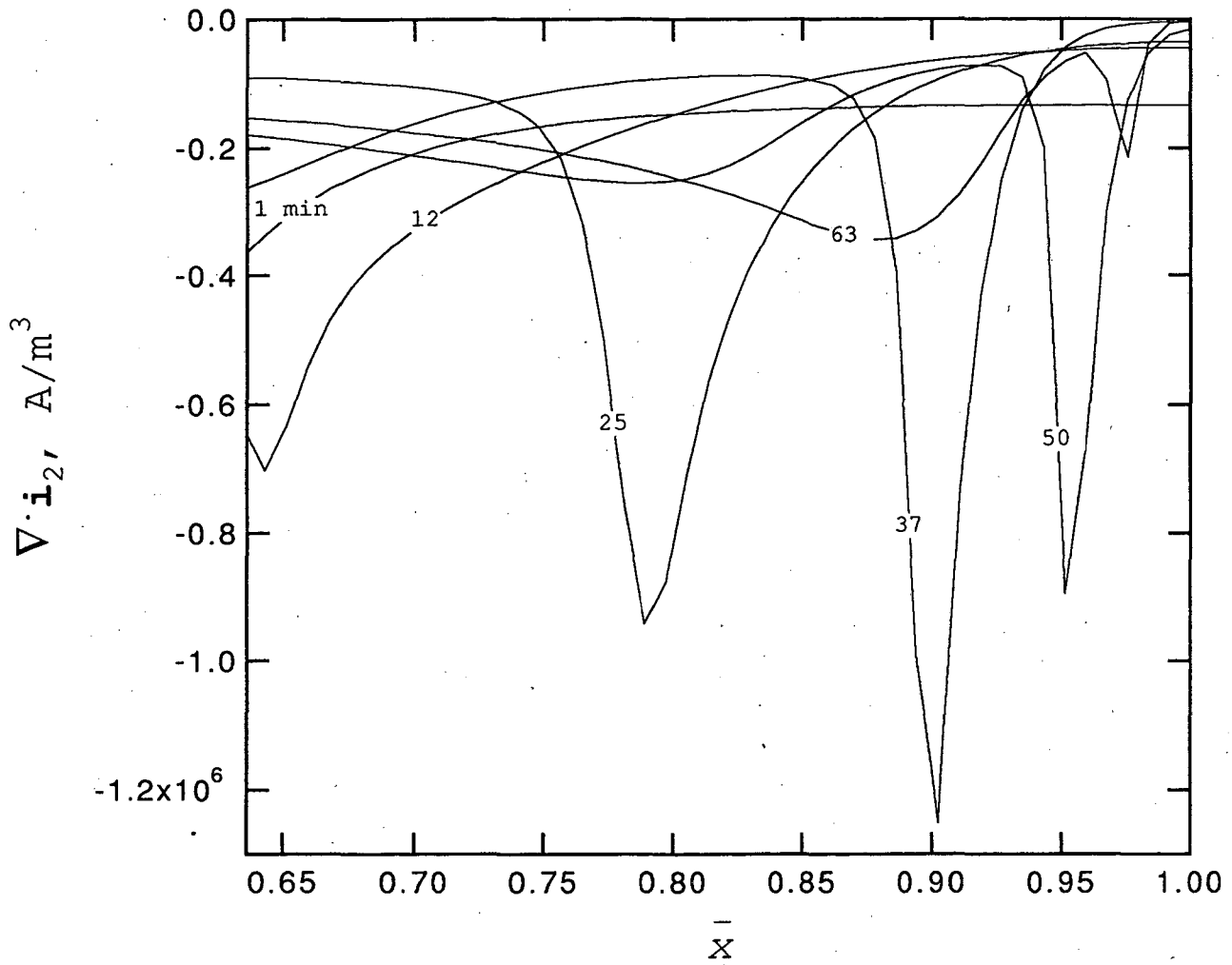


Figure 6. Divergence of solution-phase current density, which is proportional to the pore wall flux of lithium into the positive-electrode active material, during galvanostatic discharge at $I = 40 \text{ A/m}^2$. Time since the beginning of discharge is given in minutes:

sion and the transport properties. In addition, in insertion systems, the dependence of the open-circuit potential on the state of charge has an appreciable effect on the current distribution. This effect has been observed in other systems with a similar dependence of open-circuit potential on concentration. A strong dependence of open-circuit potential on concentration causes a more nearly uniform current distribution. This is analogous to the effect of the kinetic resistance on the current distribution. In contrast, systems like manganese dioxide, which exhibit a "flat" open-circuit potential, tend to have nonuniform current distributions, often resulting in a spike-shaped reaction front moving through the electrode.

With this in mind, we can explain some of the general features of figure 6. The open-circuit potential versus state of charge for the carbon and manganese dioxide materials used in this work is given for reference as figures 11 and 12. Initially ($t=1$ minute), we have the distribution skewed towards the front of the electrode, characteristic of an ohmically dominated system with the ionic conductivity of the solution much lower than the electronic conductivity of the solid phase. Then, as the active material at the front of the electrode becomes exhausted, a spike of current develops and moves across the electrode. This spike reaches the back face of the electrode when the overall utilization is about 60%, which corresponds to the end of a flat section on the open-circuit potential curve for manganese dioxide. After this, the distribution is briefly more uniform, as the open-circuit potential becomes more sloped with state of charge in this region. Then, as the open-circuit potential again levels off, another smaller spike develops.

and moves across the electrode consuming the remaining active material. It is interesting to note that a similar current distribution, involving two successive spikes moving through the porous electrode, has been predicted for the LiAl/FeS cell.⁷ There are two possible positive-electrode reactions in the iron sulfide electrode, having slightly displaced open-circuit potentials.

The current distribution in the carbon electrode is not presented because it quickly becomes uniform. Initially it is also skewed towards the front of the electrode, representing the dominance of ohmic effects. At later times the distribution is uniform, which agrees with the analysis above because the open-circuit potential of carbon is strongly dependent on the state of charge. The current distributions are similar to those seen in the titanium disulfide electrode,¹⁶ which has a similar dependence of open-circuit potential on state of charge.

Figure 7 shows the local utilization (y or x), which is proportional to the average concentration of lithium in the solid phase of each electrode. This figure allows one to examine the relationship between electrode thickness and active-material utilization. Local utilization in the carbon electrode is nearly uniform. This was supported earlier by the discussion of the current distribution in this electrode. In contrast, the local utilization in the manganese dioxide electrode is complex. This is a result of the general shape of the open-circuit potential function and also extreme concentration polarization in the electrolyte. Much of the analysis on figure 6 for the current distribution in the manganese dioxide electrode can be reexamined and confirmed using this figure. It is apparent from this figure

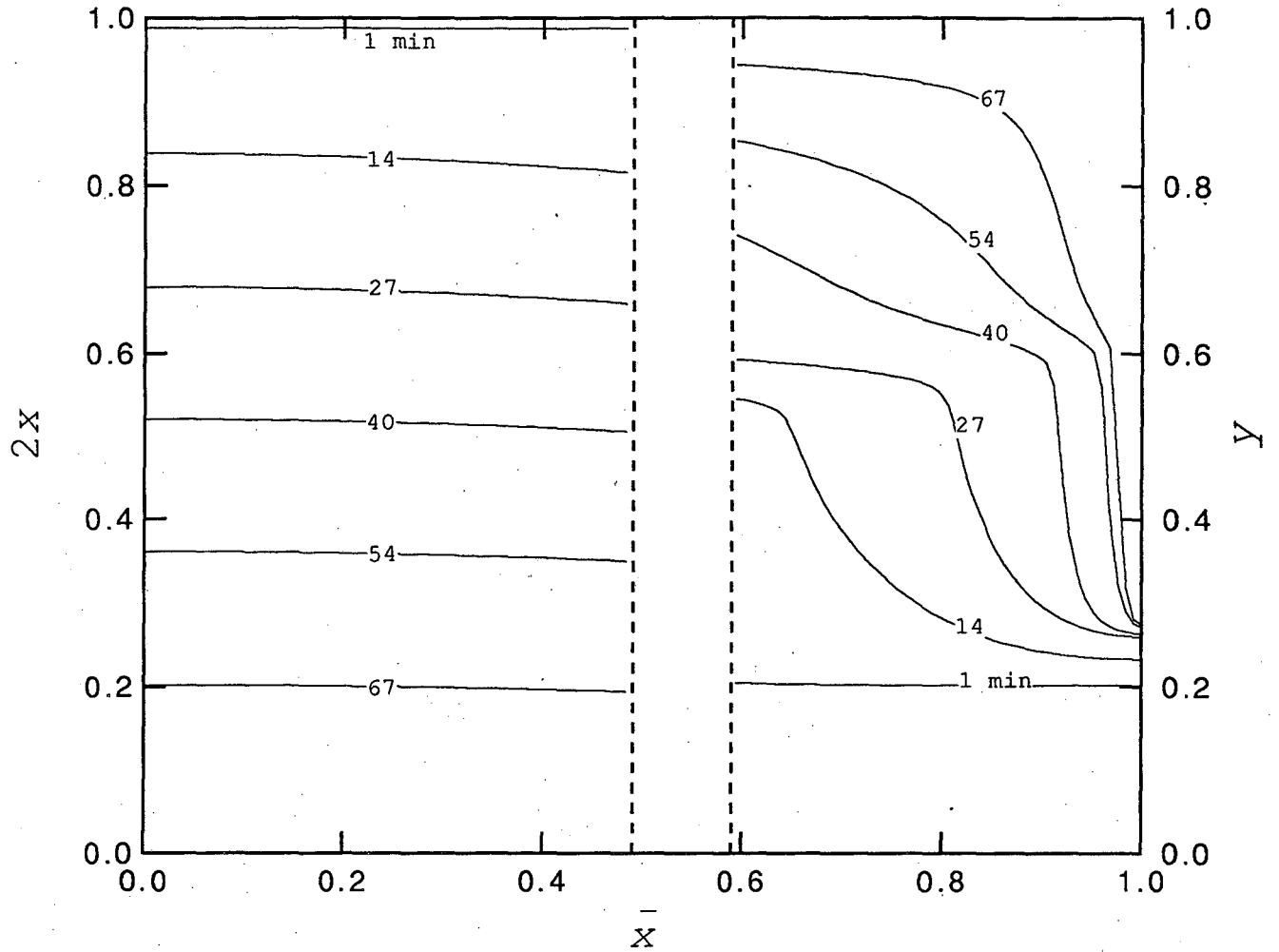


Figure 7. Local utilization of active material across the full cell during galvanostatic discharge at $I=40 \text{ A/m}^2$ for the carbon/manganese dioxide system. Time of discharge is given in minutes. Lithium deinserts from the carbon (x decreases) and inserts into the manganese dioxide on discharge.

that the material near the back face of the positive electrode is not fully utilized in this system.

Finally, we examine the the power and energy density for the carbon/manganese dioxide system. These densities are based on the mass of both composite electrodes and the separator, but not on other battery components such as current collectors, terminals, and casing. Densities of the active materials used in these simulations are given in table 1. The density of the electronically conducting filler and inert separator materials are both taken to be 2000 kg/m^3 . Figures 8 and 9 (Ragone-type plots) show the effect of electrode thickness and porosity on the performance of the system. At low current densities, the energy density approaches a theoretical limit, which is a function of the open-circuit potential. Lines representing several discharge times are also shown on these figures. Three hours corresponds to the usual time for discharge of electric-vehicle batteries.

First, we consider the effect of electrode thickness on the performance of the system. The capacity ratio for the two electrodes was kept constant here; thus, as the thickness of the positive electrode is varied, the negative electrode is always 1.21 times thicker. The porosities of the two electrodes are also kept constant and equal to the values used in the preceding simulations. Figure 8 exhibits the usual tradeoff between power and energy densities when thickness is varied. For thin electrodes a large power density is attainable, but the maximum energy density suffers as the mass of the separator becomes an appreciable fraction of the battery mass. This latter effect is only slightly apparent on figure 8 because the separator used here is thin, but it

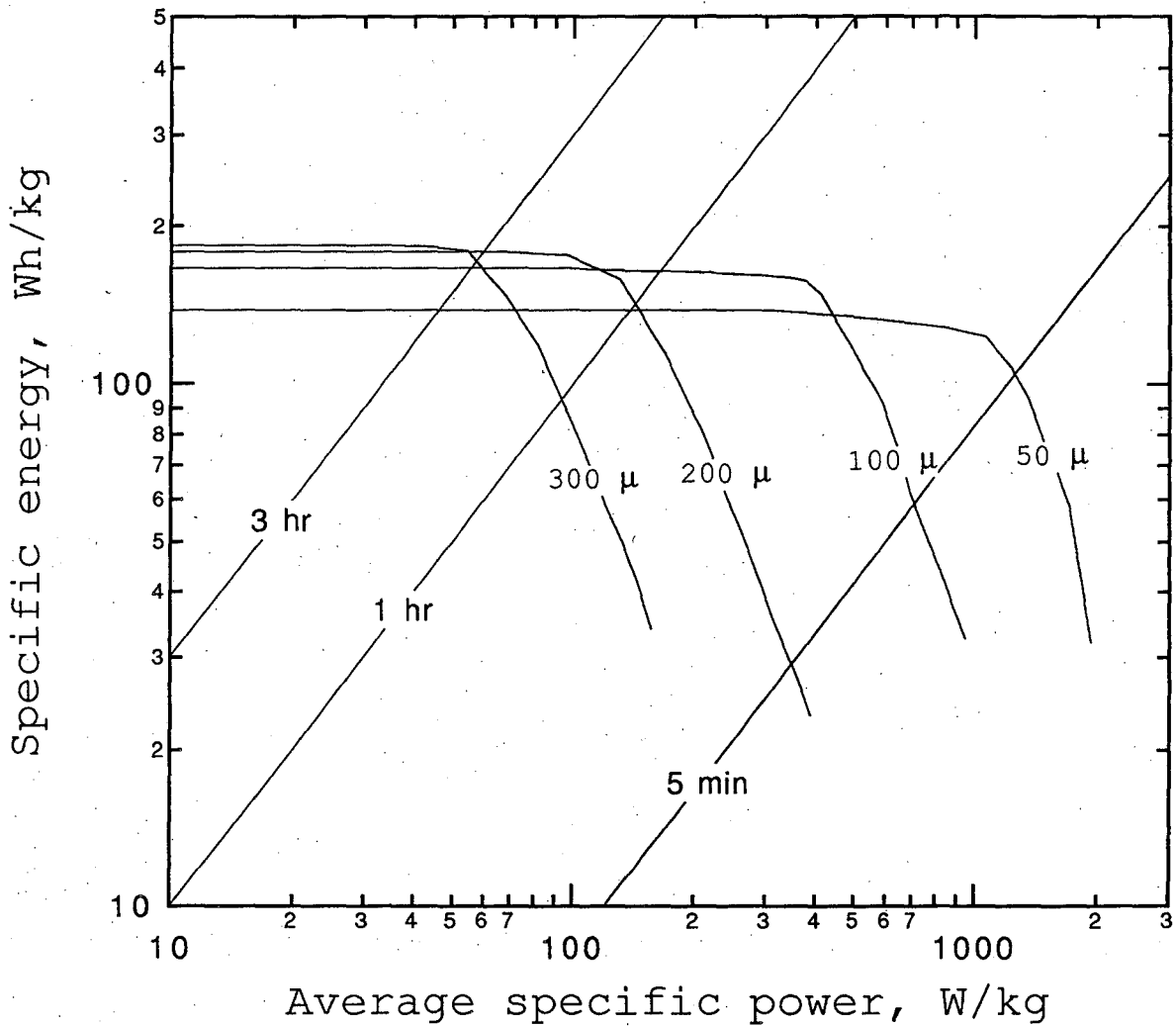


Figure 8. Ragone plot for the manganese dioxide/carbon system. The thickness of the cathode is a parameter while the porosities and ratio of capacities of the two electrodes are kept constant. Other parameters used in the simulation are given in tables 1 and 2.

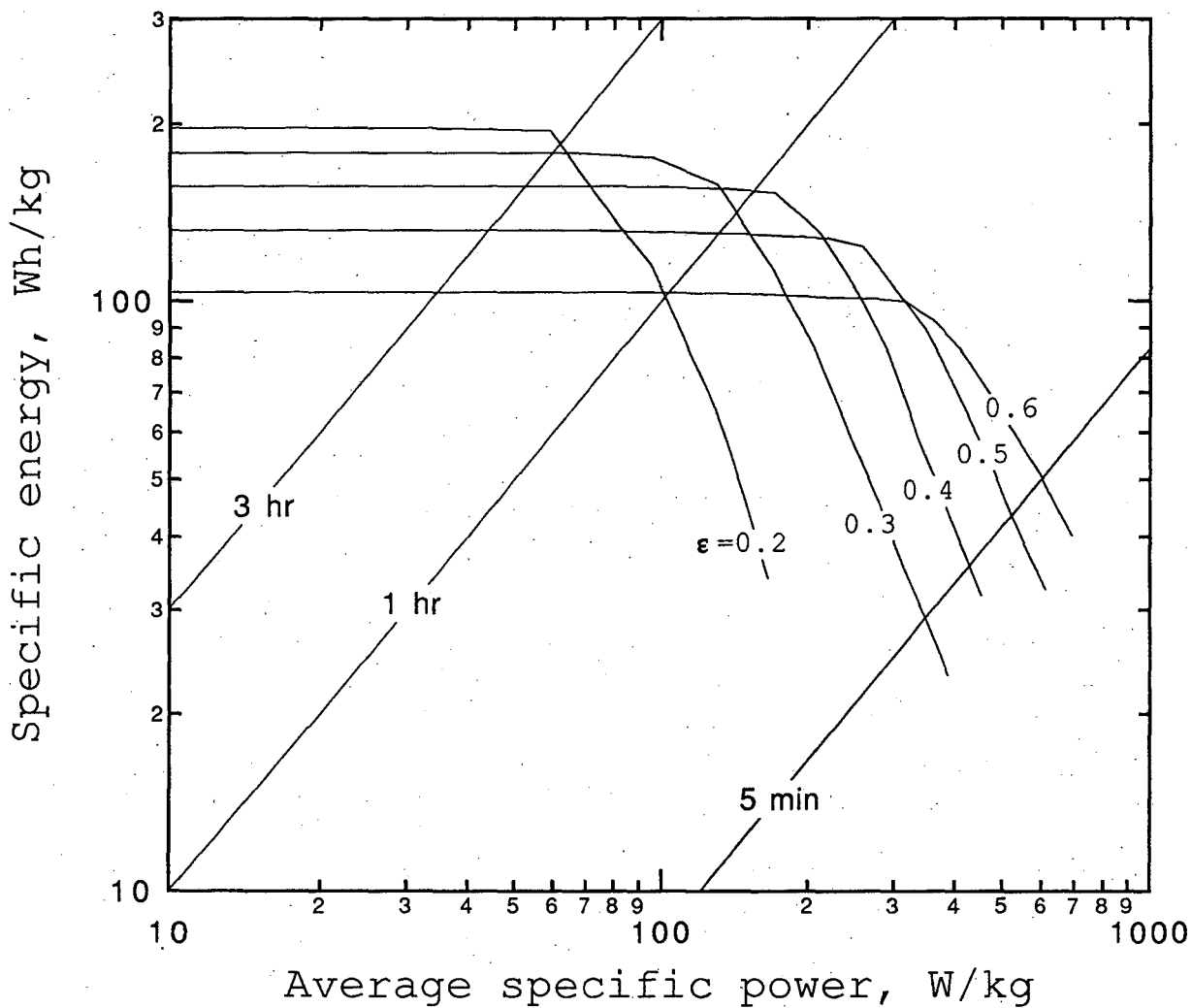


Figure 9. Ragone plot for the manganese dioxide/carbon system. The porosity of the cathode (shown as a parameter) and that of the anode vary while the thicknesses and ratio of capacities of the two electrodes are kept constant. Other parameters used in the simulation are given in tables 1 and 2.

would be accentuated if the other battery components were included in calculating the mass.

It is interesting to compare this figure with one given by Guyomard and Tarascon²² (figure 21) for the realizable specific energy and power of this system. Guyomard and Tarascon obtained their numbers by multiplying their experimental values (based on the mass of active material only) by a 33% hypothetical realization factor, a common rule of thumb. One must keep in mind that our numbers are still only theoretical values, which account for the modeling predictions of polarization effects but do not account for additional battery masses, and hence they could also be multiplied by some correction factor to account for additional battery masses. Comparing the figures, one immediately sees the similarity between results. For a particular thickness, such as 200 μm (see figure 8), the predicted power at which the realizable energy begins to fall off from its theoretical asymptote is about three times the value obtained by Guyomard and Tarascon. It is necessary to interpolate when making these comparisons because different thicknesses were used in the two cases. However, the general trend of these plots is similar as the thickness is varied over the same range of values.

One scheme for optimizing the performance of the system would be to generate curves such as figures 8 and 9 while varying different system parameters. If one had in mind minimum values of the specific energy and power for a particular application, ranges of parameters that obtain these criteria could then be identified. In general, the optimization process would be a complex one, as a multiple-parameter space would have to be explored to find the best compromise between attainable energy and

power density.²⁴ Figure 9 demonstrates the effect of varying the porosities of both electrodes while holding their thicknesses constant and equal to the values in table 2. The ratio of capacities of the two electrodes is held constant, and the porosity of the filler is constant. This graph also exhibits a tradeoff of power and energy as the relative mass of the separator increases. From this graph, one could pick an optimum porosity to use, depending on the performance guidelines one had in mind for the system.

One last comparison that is of some importance involves assessing the general effect of the additional carbon added to the anode on the performance of the system. We have simulated the performance of the system given in table 1 using a solid lithium anode instead of a carbon insertion material. The performance of these two systems is compared in figure 10. Two major reasons for using an insertion material instead of solid lithium are the growth of dendrites and film formation at the lithium surface. The film represents an irreversible loss of material and an additional ohmic drop, and would decrease the reversibility of the surface on extended cycling. Films have also been shown to form on the carbon surface, but this does not seem to have as detrimental an effect on discharge and extended cycling capabilities. As our model does not allow for film formation or dendrites, the effects of these phenomena do not appear in the results given in figure 10. Figure 10 shows that the solid lithium system exhibits both better power and energy characteristics. The theoretical energy of the solid lithium system is about 60% higher than that of the dual lithium ion insertion system owing to a higher open-circuit potential and a lower total mass. The

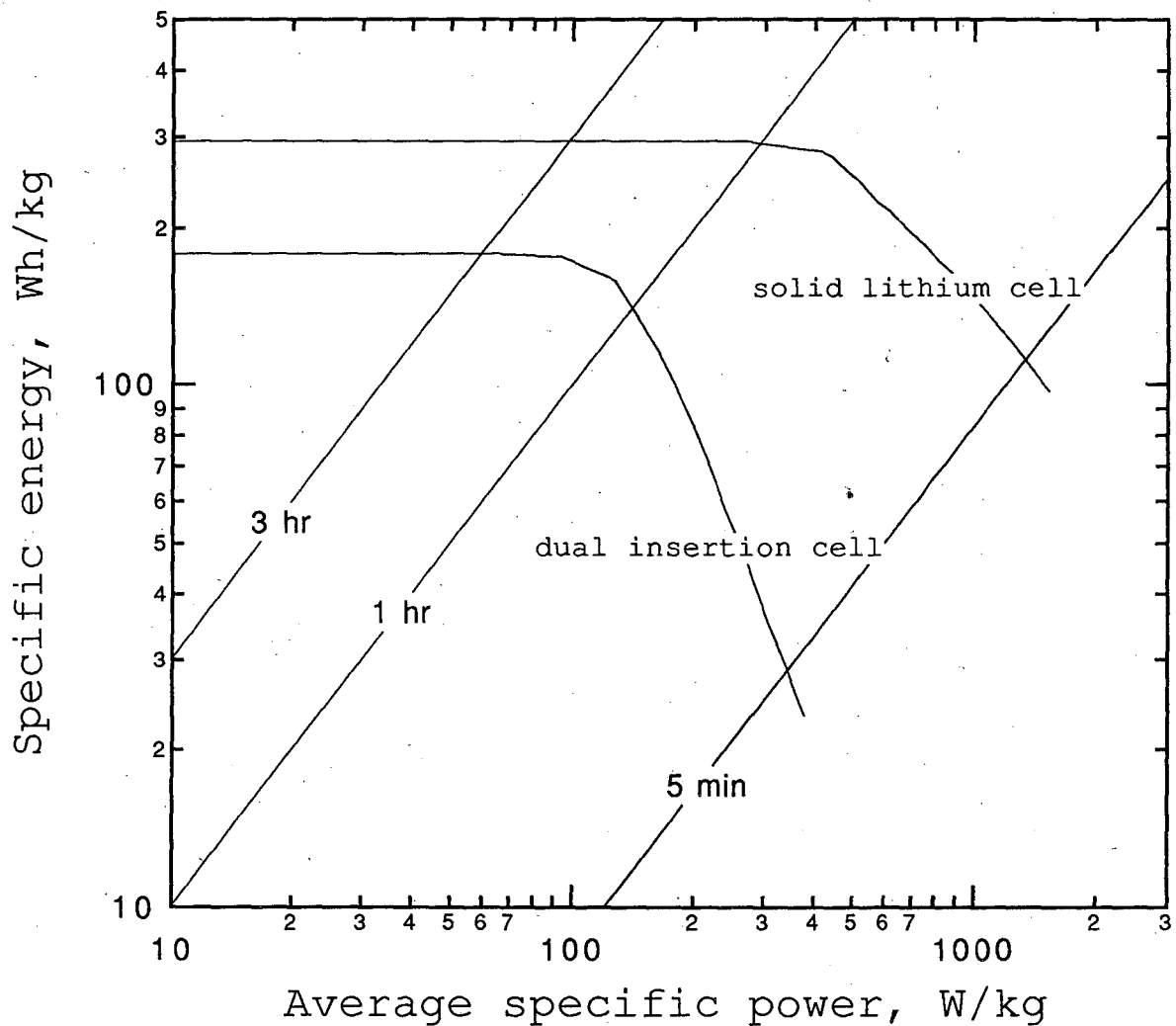


Figure 10. Comparison of Ragone plots for the dual insertion and solid lithium electrode systems. The systems are identical except for the negative electrode. The solid lithium at full charge has four times the capacity required according to stoichiometry. Other parameters used in the simulation are given in tables 1 and 2.

mass used for the solid lithium electrode corresponded to four times the stoichiometric amount required for full discharge, which is still significantly less than the mass of the composite carbon electrode.

One conclusion that can be drawn from this comparison involves the maximum concentration of salt reached in the cell in either case. We have already seen that a higher initial salt concentration improves the performance of the system, as long as the concentration of salt does not exceed the maximum concentration prescribed by a solubility limit. It is then interesting to compare the maximum salt concentrations reached in either cell, as a lower maximum would be advantageous. We find that a higher salt concentration is reached in the dual lithium ion insertion cell than when using a solid lithium electrode for a given discharge rate. For example, discharge rates above 50 A/m^2 cause the concentration to exceed the solubility limit of 2100 mol/m^3 in the dual insertion system simulated earlier. For the solid lithium system, the maximum concentration reached in the cell at this discharge rate is only 1700 mol/m^3 . Concentration depletion is also less of a problem in the solid lithium cell, with the minimum concentration at the 50 A/m^2 rate being about 350 mol/m^3 , instead of zero as in the dual insertion cell.

Summary

A model is presented for predicting the discharge behavior of dual insertion cells. The model is general and can be used to simulate any cell utilizing two composite electrodes composed of a mixture of active insertion material, electrolyte, and inert conducting material. For example, we have demonstrated, here and in reference 16, the ability to

treat Li and Li_xC_6 negative electrodes, liquid and solid polymer electrolytes, and TiS_2 and Mn_2O_4 positive electrodes. Other positive electrodes of interest include CoO_2 , V_2O_5 , V_6O_{13} , and the next plateau of Mn_2O_4 . Transport properties, thermodynamic data, and cell specifications, integral to the simulation of these systems, are detailed. The utility of the model is presented for one particular system, the carbon/manganese dioxide cell with a solution of lithium perchlorate in propylene carbonate. Discharge curves are presented for various current densities, and the major process limiting high rates of discharge in this system is found to be the increase in concentration overpotential because of depletion of the electrolyte. An analysis of the current distribution in these systems shows the importance of the rate of change of the open-circuit potential of the insertion material with the state of charge.

The optimization of these systems for a particular application has been discussed in terms of the attainable power and energy densities. The lithium ion dual insertion systems exhibit the large theoretical specific energy densities hoped for with lithium based systems, although the energy is necessarily reduced from corresponding systems utilizing solid lithium anodes. The attainable power is also large, making thin cells ideally suited for high-rate-of-discharge applications such as acceleration of electric-vehicles. The energy and power densities quoted here represent simulated values, not accounting for losses due to extended cycling or additional battery mass. Yet even as such, the performance of these systems is promising, and it is likely that these cells will command an increasing amount of interest in the future.

Acknowledgements

This work was supported by the Assistant Secretary for Conservation and Renewable Energy, Office of Transportation Technologies, Electric and Hybrid Propulsion Division of the U. S. Department of Energy under Contract No. DE-AC03-76SF00098.

Appendix A Transport properties of the electrolyte and thermodynamic data

Propylene carbonate, 1 M LiClO₄. — The concentration dependence of the conductivity was fit from available data of Gores and Barthel.²³ The diffusion coefficient of the salt¹⁵ ($D=2.58 \times 10^{-10} \text{ m}^2/\text{s}$) and transference number of lithium²⁵ ($t_+^0=0.2$) were taken to be constant, since reproducible data were not available. Activity coefficient data have not been reported.

Electrode thermodynamic data. — The open-circuit potential versus state of charge for manganese dioxide²⁶ was fit to the function

$$\begin{aligned}
 U^\theta = & 4.06279 + 0.0677504 \tanh[-21.8502y + 12.8268] \\
 & - 0.105734 \left[\frac{1}{(1.00167-y)^{0.379571}} - 1.576 \right] \\
 & - 0.045 \exp(-71.69y^8) + 0.01 \exp[-200(y-0.19)],
 \end{aligned}
 \tag{A-1}$$

where y is the amount of lithium inserted in $\text{Li}_y\text{Mn}_2\text{O}_4$. This curve fit is given as figure 11. Similarly, for the carbon electrode⁹

$$U = -0.132 + 1.41 \exp(-3.52x),
 \tag{A-2}$$

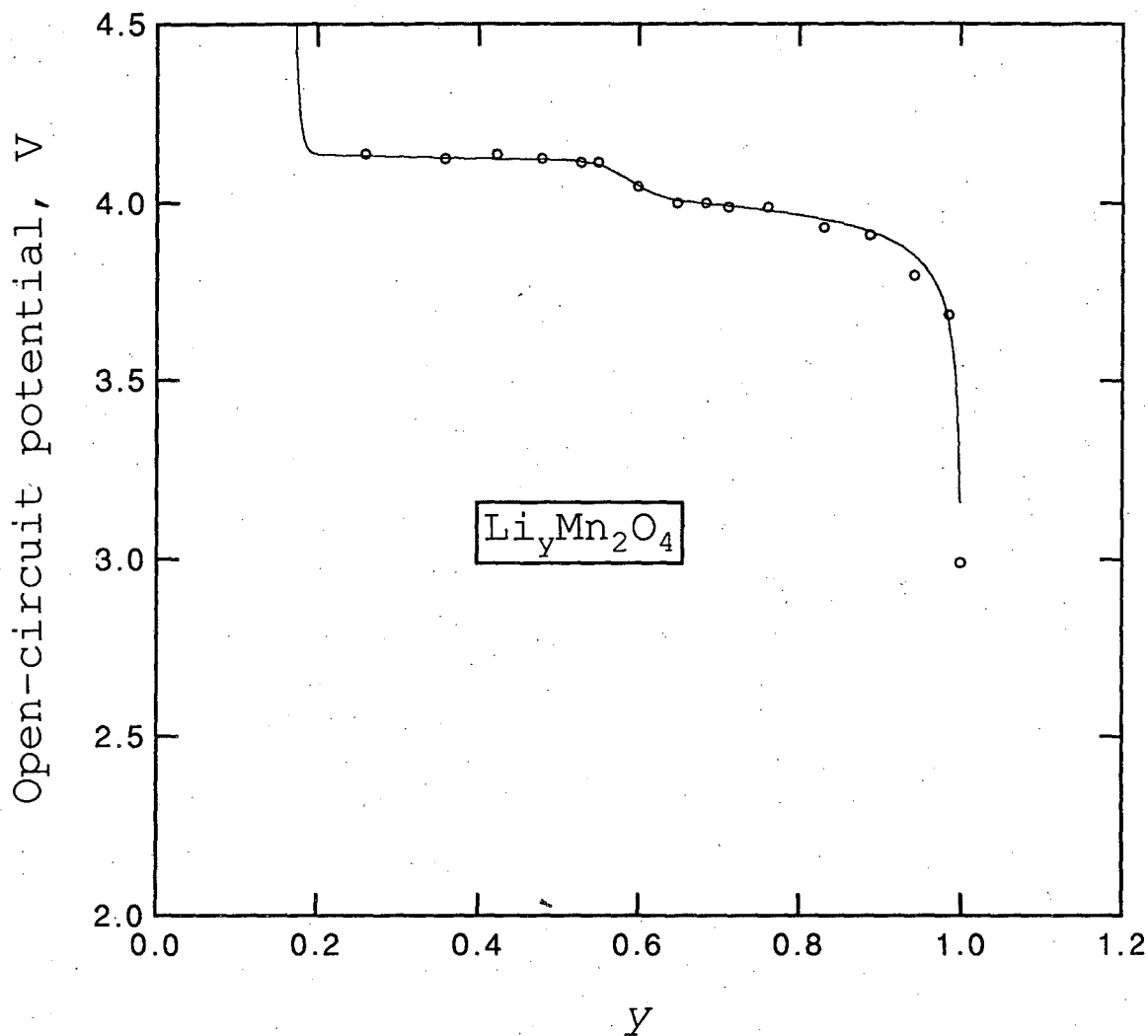


Figure 11. The open-circuit potential of manganese dioxide as a function of the state of charge relative to the potential of solid lithium at the same electrolyte concentration. Data reported by Ohzuku et al.²⁶

where x is the value defined by the formula Li_xC_6 . Open-circuit-potential data were not available for this system, and the above function corresponds to the potential of carbon versus lithium during a low-current discharge. However, this is expected to resemble closely the open-circuit potential under these conditions (low discharge rate). This fit is presented as figure 12.

Appendix B Superposition

Since the equations describing transport in the active cathode material are linear, contributions to the flux from a series of step changes in surface concentration can be superposed. This is an example of Duhamel's superposition integral:²⁰

$$\frac{\partial c_s}{\partial r}(R_s, t) = \int_0^t \frac{\partial c_s}{\partial t}(R_s, \zeta) \frac{\partial \bar{c}_s}{\partial r}(R_s, t-\zeta) d\zeta, \quad (\text{B-1})$$

where \bar{c}_s represents the solution to equation 10 for a unit step change in concentration at the surface. The above integral is calculated numerically using the method suggested by Wagner²⁷ and by Acrivos and Chambré.²⁸ Whence,

$$\frac{\partial c_s}{\partial r}(R_s, t) = \sum_{k=0}^{n-2} \left[\frac{c_{s,k+1} - c_{s,k}}{\Delta t} \right] A_{n-k} + \left[\frac{c_{s,n} - c_{s,n-1}}{\Delta t} \right] A_1, \quad (\text{B-2})$$

where

$$A_{n-k} = a[(n-k)\Delta t] - a[(n-k-1)\Delta t] \quad (\text{B-3})$$

and

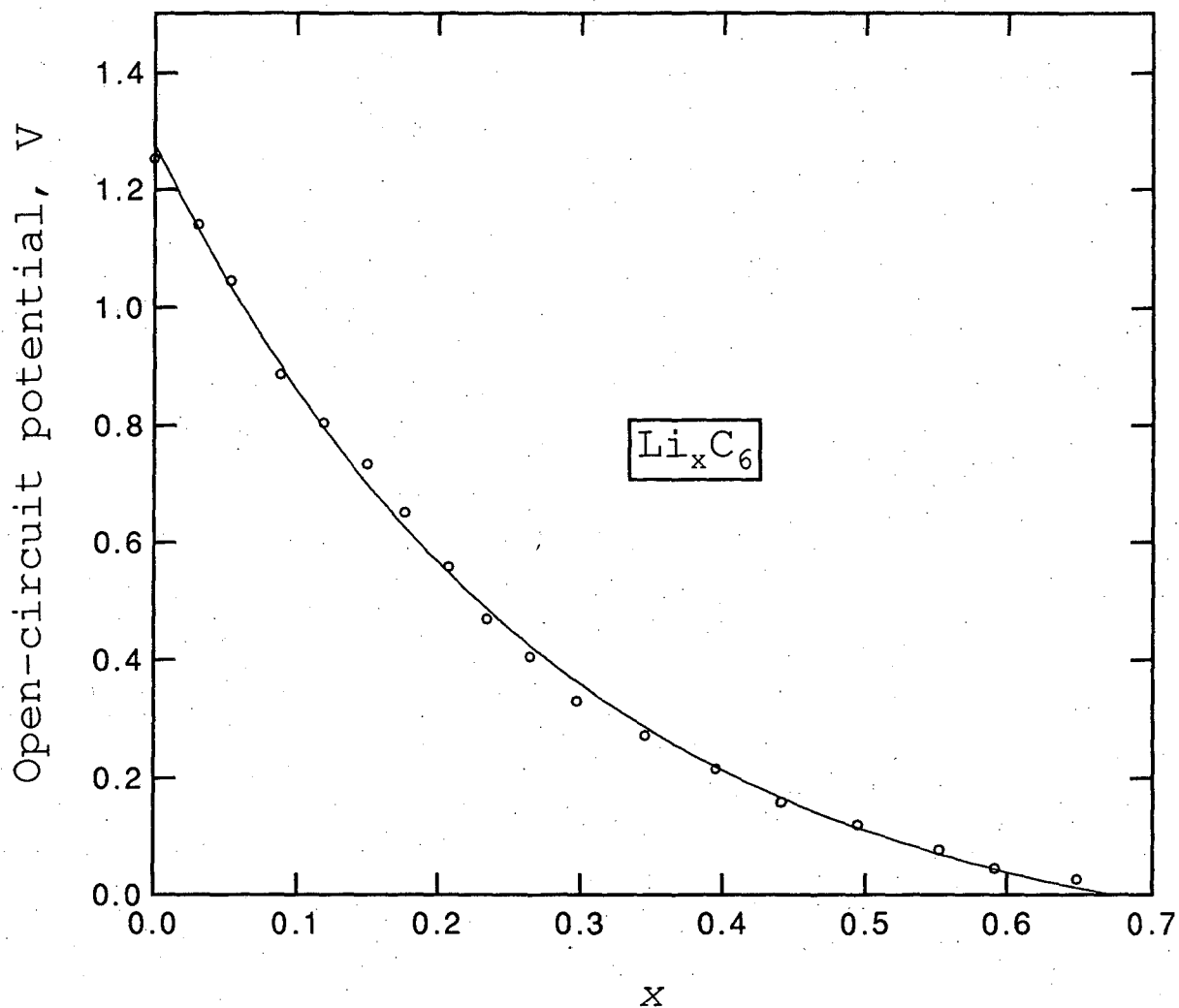


Figure 12. The open-circuit potential of carbon (petroleum coke) as a function of state of charge relative to the potential of solid lithium at the same electrolyte concentration. Data reported by Fong et al.⁹

$$a(t) = \int_0^t \frac{\partial \bar{c}_s}{\partial r}(R_s, \zeta) d\zeta. \quad (\text{B-4})$$

By means of Laplace transforms, two expressions for $a(t)$ were developed: at long times,

$$a(\tau) = \frac{2}{\pi^2} \sum_{n=1}^{\infty} \frac{1}{n^2} \left[1 - \exp\left(-n^2 \pi^2 \tau\right) \right], \quad (\text{B-5})$$

and for short times

$$a(\tau) = -\tau + 2 \left(\frac{\tau}{\pi}\right)^{1/2} \left[1 + 2 \sum_{n=1}^{\infty} \exp\left(\frac{-n^2}{\tau}\right) - n \left(\frac{\pi}{\tau}\right)^{1/2} \operatorname{erfc}\left(\frac{n}{\sqrt{\tau}}\right) \right]. \quad (\text{B-6})$$

τ is dimensionless time; $\tau = tD_s/R_s^2$. These expressions are each uniformly valid; however, the latter expression converges much more quickly with fewer terms at very short times. The values of $a(\tau)$ and A_{n-k} can be calculated separately and used whenever equation B-2 needs to be evaluated. This procedure, applicable for a constant diffusion coefficient, is consequently more efficient than solving for the two-dimensional transport directly.

List of Symbols

a	specific interfacial area, m^2/m^3
c	concentration of electrolyte, mol/m^3
c_i	concentration of species i , mol/m^3
D, D_s	diffusion coefficient of electrolyte and of lithium in the solid matrix, m^2/s

f_{\pm}	activity coefficient
F	Faraday's constant, 96,487 C/eq
i	current density, A/m ²
i_0	exchange current density, A/m ²
I	superficial current density, A/m ²
j_n	pore wall flux across interface, mol/m ² ·s
k	reaction rate constant
K_{ij}	frictional coefficient, J·s/m ⁵
L	thickness of cell, m
n	number of electrons transferred in electrode reaction
N_i	molar flux in x direction of species i , mol/m ² ·s
r	radial distance in a particle of active material, m
R	universal gas constant, 8.3143 J/mol·K
R_s	radius of cathode material, m
s_i	stoichiometric coefficient of species i in electrode reaction
S_s, S_e	dimensionless ratios defined in equations 19 and 20
t	time, s
t_i^0	transference number of species i
T	temperature, K
U	open-circuit potential, V
v_i	velocity of species i , m/s
V	cell potential, V
x	distance from the negative electrode current collector, m
\bar{x}	dimensionless distance
z	capacity ratio of positive to negative electrode
z_i	charge number of species i

α_a, α_c	transfer coefficients
δ_s	thickness of separator, m
δ_+	thickness of composite positive electrode, m
δ_-	thickness of composite negative electrode, m
ϵ	porosity
η	overpotential, V
κ	conductivity of electrolyte, S/m
ν	dimensionless exchange current density
ν_+, ν_-	number of cations and anions into which a mole of electrolyte dissociates
ρ	density, kg/m ³
σ	conductivity of solid matrix, S/m
τ	dimensionless time
μ_i	electrochemical potential of species i , J/mol
Φ	electrical potential, V

Subscripts

e	electrolyte
f	filler
ref	reference state
s	solid phase or separator
1	solid matrix
2	solution phase
t	concentration in intercalation material for $y=1$
+	positive electrode
-	negative electrode

Superscripts

0	solvent, or initial condition
θ	standard cell potential

References

[1] E. J. Cairns, "A New Opportunity for Electrochemical Energy Conversion," *Interface*, 1, 38-39 (1992).

[2] Bruno Scrosati, "Lithium Rocking Chair Batteries: An Old Concept?" *J. Electrochem. Soc.*, 139, 2776-2781 (1992).

[3] Sony's Lithium Manganese Rechargeable Battery (AA Size), *JEC Press, Inc.*, p. 26 (February, 1988).

[4] Moli Energy's New Product Data Sheet, *JEC Battery Newsletter*, No. 6, p. 15 (Nov-Dec, 1988).

[5] Sanyo's Lithium Rechargeable Battery, *JEC Battery Newsletter*, No. 3, p. 15 (1989).

[6] D. Aurbach, M. L. Daroux, P. W. Faguy, and E. Yeager, "Identification of Surface Films Formed on Lithium in Dimethoxyethane and Tetrahydrofuran Solution," *J. Electrochem. Soc.*, 135, 1863-1871 (1988).

[7] R. Pollard and J. Newman, "Mathematical Modeling of the Lithium-Aluminum, Iron Sulfide Battery," *J. Electrochem. Soc.*, 128, 491 (1981).

[8] K. M. Abraham, D. M. Pasquariello, and E. B. Willstaedt, "Preparation and Characterization of Some Lithium Insertion Anodes for Secondary Lithium Batteries," *J. Electrochem. Soc.*, 137, 743 (1990).

[9] R. Fong, U. von Sacken, and J. R. Dahn, "Studies of Lithium Intercalation into Carbons Using Nonaqueous Electrochemical Cells," *J. Electrochem. Soc.*, 137, 2009 (1990).

[10] M. S. Whittingham and A. J. Jacobson, eds., *Intercalation Chemistry*, Academic Press, New York (1982).

[11] M. S. Whittingham, "The Role of Ternary Phases in Cathode Reactions," *J. Electrochem. Soc.*, 123, 315 (1976).

[12] J. Desilvestro and O. Haas, "Metal Oxide Cathode Materials for Electrochemical Energy Storage: A Review," *J. Electrochem. Soc.*, 137, 5C (1990).

[13] M. Lazzari and B. Scrosati, "A Cyclable Lithium Organic Electrolyte Cell Based on Two Intercalation Electrodes," *J. Electrochem. Soc.*, 127, 773 (1980).

[14] M. Armand, in *Materials for Advanced Batteries*, D. W. Murphy, J. Broodhead, and B. C. H. Steele, eds., p. 145, Plenum Press, New York (1980).

[15] K. West, T. Jacobsen, and S. Atlung, "Modeling of Porous Insertion Electrodes with Liquid Electrolyte," *J. Electrochem. Soc.*, 129, 1480 (1982).

[16] M. Doyle, T. F. Fuller, and J. Newman, "Modeling of the Galvanostatic Charge and Discharge of the Lithium/polymer/insertion Cell," *J. Electrochem. Soc.*, 140, 1526 (1993).

[17] John Newman, *Electrochemical Systems*, Prentice-Hall, Englewood Cliffs, New Jersey (1991).

[18] T. F. Fuller and J. Newman, "Experimental Determination of the Transport Number of Water in Nafion 117 Membrane," *J. Electrochem. Soc.*, 139, 1332 (1992).

[19] R. E. Meredith and C. W. Tobias, "Conduction in Heterogeneous Systems," in *Advan. Electrochem. Electrochem. Eng.*, C. W. Tobias, ed., 2, 15 (1962).

[20] F. B. Hildebrand, *Advanced Calculus for Applications*, p. 463, Prentice-Hall Inc., Englewood Cliffs, New Jersey (1976).

[21] R. Pollard and J. Newman, "Transient Behaviour of Porous Electrodes with High Exchange Current Densities," *Electrochim. Acta*, 25, 315 (1980).

[22] D. Guyomard and J. M. Tarascon, "Li Metal-free Rechargeable LiMn_2O_4 Carbon Cells: Their Understanding and Optimization," *J. Electrochem. Soc.*, 139, 937-948 (1992).

[23] H. J. Gores and J. Barthel, "Conductance of Salts at Moderate and High Concentrations in Propylene Carbonate-Dimethoxyethane Mixtures at Temperatures from -45°C to 25°C ," *J. of Solution Chem.*, 9, 939-954 (1980).

LAWRENCE BERKELEY LABORATORY
UNIVERSITY OF CALIFORNIA
TECHNICAL INFORMATION DEPARTMENT
BERKELEY, CALIFORNIA 94720

ABH387

LBL Libraries